Citation for published version:
Akinbade, Y, Harries, KA, Flower, CV, Nettleship, I, Papadopoulos, C & Platt, S 2019, 'Through-culm wall mechanical behaviour of bamboo', *Construction and Building Materials*, vol. 216, pp. 485-495.
https://doi.org/10.1016/j.conbuildmat.2019.04.214

DOI:
10.1016/j.conbuildmat.2019.04.214

Publication date:
2019

Document Version
Peer reviewed version

Link to publication

Through-Culm Wall Mechanical Behaviour of Bamboo

Yusuf Akinbade[1], Kent A. Harries[2], Chelsea V. Flower[3], Ian Nettleship[4], Christopher Papadopoulos[5] and Shawn Platt[6]

Abstract

Performance of full-culm bamboo structures is dominated by longitudinal splitting behaviour, often exacerbated by connection details. This behaviour is a function of the transverse properties of this highly orthotropic material. Considerable study of the longitudinal properties of bamboo is available in which it is often concluded that bamboo may be considered as a fibre-reinforced composite material and material properties may be assessed using rule-of-mixture methods. Nonetheless, few studies have addressed the transverse properties of the bamboo culm wall, despite these largely governing full-culm behaviour. This study investigated the transverse material property gradient through the culm wall and attempts to connect the mechanical results to physical observations and phenomena. Most importantly, the study demonstrates that the complex transverse behaviour of bamboo does not appear to behave as a classic fibre-reinforced composite material in the direction transverse to the fibres. In this study, five different bamboo species, *Phyllostachys edulis*, *Phyllostachys bambusoides*, *Phyllostachys meyeri*, *Phyllostachys nigra*, and *Bambusa stenostachya* were tested using a modification of the flat-ring flexure test to obtain a measure of the transverse tensile capacity of the bamboo. Microscopy analyses are used to qualitatively describe the culm wall architecture and to quantitatively assess the failure modes through the culm wall thickness.

Keywords

bamboo; fibre gradient; fibre volume; material testing; rule of mixtures; splitting

1. Introduction

A functionally graded, natural fibre-reinforced material [Ghavami et al 2003], bamboo has evolved in nature to efficiently resist environmental loads. Bamboo has been shown to have mechanical properties comparable to those of conventional building materials and its worldwide availability gives it great potential as an alternative building material. Rapid growth (mature in 3 to 5 years followed by a 2 to 3 year harvest cycle), very low fertilizer requirement (typically none) and the ability to replace conventional

---

[1] PhD candidate, Department of Civil and Environmental Engineering, University of Pittsburgh

[2] Bicentennial Board of Visitors Faculty Fellow and Professor, Department of Civil and Environmental Engineering, University of Pittsburgh; kharries@pitt.edu

[3] Undergraduate Research Fellow, Department of Civil and Environmental Engineering, University of Pittsburgh

[4] Associate Professor, Department of Materials and Mechanical Engineering, University of Pittsburgh

[5] Associate Professor, Department of Civil and Engineering, University of Puerto Rico at Mayaguez

[6] Post doctoral Researcher, University of Bath, United Kingdom.

materials that are resource and energy intensive, combine to make bamboo a potentially sustainable material in terms of both ‘carbon footprint’ and social equity. Bamboo offers versatility for use in a broad range of international contexts, from use as an affordable and sustainable material in developing countries to rapidly-deployable structures for disaster relief, to mainstream or niche construction in wealthier countries.

The structure of bamboo is composed of culms (stalks) with solid transverse diaphragms or ‘nodes’ separating hollow inter-nodal regions along its height (Figure 1a). The circular cross section (Figures 1b-d) is composed of unidirectional cellulosic fibres oriented parallel to the culm’s longitudinal axis embedded in a parenchyma tissue matrix [Grosser and Liese 1971]. The parenchyma tissue matrix lignifies (hardens) as the culm matures leading to increased density and improved mechanical properties. As a functionally graded material, bamboo has evolved to resist its primary loading in nature: its own self-weight and the lateral effects of wind. As seen in Figure 1c, the density of fibres increases from the inner culm wall to the outer culm wall. The wall thickness is largest at the base of the culm and decrease with height up the culm. However, the size and quantity of vessels decrease with the height of the culm and are replaced with bamboo fibres. This addition of fibres compensates for loss in strength and stiffness due to reductions in diameter and wall thickness near the top of the culm, resulting in relatively uniform engineering properties along the entire culm height [Amada 1996; Harries et al. 2017]. Like any fibre-reinforced material, mechanical properties are highly correlated to the proportion and distribution of fibres in the cross section. Mechanical properties are influenced by density, which depends on fibre content, fibre diameter, and cell wall thickness [Janssen 2000]. The density of most bamboo is 700 – 800 kg/m^3 depending on species, growing conditions, and position along the culm. The volume fraction of fibres ranges from approximately 60% at the exterior face of the culm wall to 10-15% near the interior face (Figure 1c). The variation in density through the culm wall has been assumed by various researchers to be linear, quadratic, exponential, or a power function and is known to be species-dependent [Amada et al. 1996 and 1997]. Table 1 summarises fibre volume distributions reported in the literature in addition to gross section and inner and outer wall fibre volume ratios (V_f) and longitudinal moduli (E_L). Due to the complex variation of the fibres and vascular bundles, the variation of material properties through the culm-wall thickness has been shown to be significant [Richard and Harries 2015] and to have the effect of increasing gross culm stiffness by about 10% as compared to an assumed uniform distribution of the same volume of fibers [Janssen 2000]. Harries et al. [2017], in a more refined analysis, showed the effect of fibre gradient on gross culm stiffness to result in about a 5% increase for thin-walled culms ($D/t < 8$) and as much as 20% for thick-walled culms ($D/t > 8$; where D is the culm outer diameter and t is the culm wall thickness).

In general, while highly variable, the longitudinal behaviour of bamboo is relatively well understood in a qualitative sense. From an engineering perspective, the longitudinal behaviour is most typically considered as a fibre-reinforced material in which longitudinal properties are obtained using a rule of mixtures approach. For example, gross section modulus, E_L, is estimated from:

$$E_L = V_f E_f + (1 - V_f) E_m \qquad \text{Eq. 1}$$

Where V_f is the fibre volume ratio and E_f and E_m are the moduli of the fibre and matrix (parenchyma) phases, respectively. Janssen (2000) reports typical values of $E_f = 35$ GPa and $E_m = 1.8$ GPa.

The dominant failure mode of bamboo, however, is longitudinal splitting associated with bamboo carrying flexure, compression or tension loads; splitting is exacerbated by the use of simple bolted connection details common in some bamboo construction [Sharma et al. 2012]. Janssen [1981] describes the bending stresses in a culm as being characterised by the longitudinal compressive stress and transverse strain in the compression zone of the culm, with failure eventually occurring due to longitudinal splitting. This is ideally a Mode II[7] longitudinal shear failure. However, in the presence of perpendicular stresses (as is the case where ever there is a non-zero shear-to-moment ratio), there is some Mode I component stress which significantly reduces the Mode II capacity. Richard et al. [2017] demonstrate the effects of such mode mixity using longitudinal shear tests [ISO 2004] which capture pure Mode II behaviour, split pin tests [Mitch et al. 2010] which capture Mode I behaviour, and culm bending tests of different spans resulting in different degrees of mode mixing. For two different species, a thin walled *P. edulis* and thick-walled *B. stenostachya*, the split pin tests resulted in Mode I capacities equal to only 18% of the Mode II capacity determined from the longitudinal shear tests. Beam tests having mixed mode behaviour exhibited shear capacities ranging from 40-70% of the Mode II capacity.

Both the Mode I and II behaviours described are primarily functions of the transverse properties of the fibre-reinforced culm which are believed to be dominated by matrix (parenchyma) properties. Despite their importance in the dominant observed behaviour of full-culm bamboo, there are few studies of the transverse properties of the culm wall. In early work, Arce-Villalobos [1993] concluded that there is no correlation between the density of bamboo and its transverse tensile strength. Janssen [2000], based on flexural tests, reports that a transverse strain of 0.0013 results in transverse tensile failure of the culm wall (with no indication of species or other variation). More recently, test methods have been proposed for obtaining transverse properties of bamboo culms [Mitch et al. 2010; Sharma et al. 2012; Virgo et al. 2017] although these have not yet been widely adopted to obtain material properties over a range of species and conditions. Sharma and Harries [2012] report a unique attempt to refine an edge bearing test to determine through culm-wall distribution of properties. In this study, the culm was cut, using a water

---

[7] Reference to Modes II and I are in relation to classical fracture mechanics in which Mode II refers to forces resulting in ‘in-plane shear’ and Mode I refers to perpendicular in-plane ‘peeling’ forces.

jet, into two or three concentric annular sections. Edge bearing test results for each resulting ‘ring’ provided an improved measure of through-thickness transverse properties than could be obtained from a single full-culm section. The approach was limited to thicker culm walls, provided only two or three data points across the culm wall and did not result in repeatable specimens and was therefore abandoned.

Tan et al. [2011] conducted a micro-scale study on the crack growth and toughening mechanisms of *P. edulis*. The study revealed that toughening was inversely related to fibre density. The authors noted that their results suggest the need to account for the anisotropic strength and fracture properties of bamboo in the design of bamboo structures.

In order to understand the transverse behaviour of bamboo, it is informative to consider laminate theory and the rule of mixtures for transverse properties:

$$E_T = [V_f/E_f + (1 - V_f)/E_m]^{-1} \qquad \text{Eq. 2}$$

Equation 2 is conventionally considered a lower-bound estimate of transverse properties since it does not account for the anisotropic nature of the fibre itself and, as a result, underestimates off-longitudinal properties [Mallick 2008]. The Halpin-Tsai equations [Halpin and Kadros 1976] are most often adopted to describe transverse behaviour of fibre-reinforced composites:

$$E_T = E_m(1 + \xi n V_f)/(1-nV_f) \qquad \text{Eq. 3}$$

Where $n = (E_f/E_m - 1)/(E_f/E_m + \xi)$ Eq. 4

The value of ξ is an empirical constant fitted to the elasticity solution for a fibre geometry and confirmed by experimental data [Halpin and Kadros 1976]:

$$\xi = 2 + 40V_f^{10} \qquad \text{Eq. 5}$$

When considering transverse properties of longitudinally reinforced fibre composites having V_f less than 0.5, it is conventional to assign $\xi = 2$ [Hewitt and de Malherbe 1970]. Halpin-Tsai is equally applicable to determining longitudinal properties. For longitudinal properties of long continuous fibre composites (such as bamboo) however, Halpin-Tsai results in the same relationship as the rule-of-mixtures (Eq. 1).

Figure 2 presents theoretical longitudinal and transverse modulus distributions determined using the rule of mixtures and Halpin-Tsai, respectively (Equations 1 and 3). The fibre volume distribution illustrated is that proposed by Dixon and Gibson [2014] for *P. edulis* and is representative of most distributions reported in Table 1. The modulus distributions shown are normalised by the average modulus for the culm wall which is what should be obtained when testing a full-culm specimen (i.e., the apparent modulus of the gross section). In addition to the variation in properties, a shift of the neutral axis of the section (at which location ratios equal unity) toward the outer culm wall is evident. This shift results in the increase in gross culm stiffness described previously [Janssen 2000; Harries et al. 2017].

The objective of the present study is to investigate the transverse material property gradient through the culm wall and to connect the mechanical results to physical results, such as fibre density. In this study, a modification to the flat-ring flexure [Virgo et al. 2017] test specimen, in which only portions of the culm wall cross-section are tested, is used to obtain a measure of the transverse tensile capacity of the bamboo. Microscopy analyses are used to qualitatively describe the culm wall architecture and to quantitatively assess the failure modes through the culm wall thickness. Throughout this study, all data is also normalised by culm wall thickness ($x = 0$ is the inner wall and $x = 1$ is the outer wall).

2. Flat-ring Flexure Test

The flat ring flexure test [Virgo et al. 2017] assesses the tendency of bamboo to fail via longitudinal cracks using a full cross-sectional specimen that is $L \approx 0.2D$ in length. The specimen is subjected to 4-point flexure as shown in Figure 3. The desired failure for this test occurs in the constant moment region. The flat ring flexure test gives the apparent modulus of rupture of the specimen (f_r) which, due to specimen geometry, is related to the transverse tension capacity of the bamboo. The modulus of rupture is calculated from the test results as:

$$f_r = 3Pa/(t_N + t_S)L^2 \qquad \text{Eq. 5}$$

Where P is total load applied to specimen; a is the shear span; t_N and t_S are culm wall thickness at the failure locations on either side of the culm; and L is the length of culm section tested (i.e., the flexural depth of specimen). A practical test span is found to be approximately $S = 0.85D$ and the shear span should be at least $0.33S$. This test is easily translated to a field setting, requiring only two loading plates, four pins, and free weights, rather than a hydraulic press. Nonetheless, in this study, all tests were carried out in a mechanically driven universal test machine. Tests are conducted in displacement control at a rate of crosshead travel of 0.76 mm/min resulting in failure in between 1 and 5 minutes. Loads are obtained using a load cell with a precision of ± 0.4N. A specimen loading apparatus (Figure 3b) is used to ensure accurate and repeatable specimen alignment. With this apparatus, test span and shear span can be varied independently in increments of 5 mm. Prior to this study, the flat-ring flexure test has been used on only full-culm cross sections. Such full-culm cross section specimens are referred to in this work as the control specimens and the modulus of rupture thus obtained is denoted f_{rC}.

2.1 Clipped Flat-ring Test Specimens

This study adopts a modification to the flat-ring test specimen, in which only portions of the cross-section are tested in order to determine the effect of the material property gradient through the culm wall. The culms were cut into full cross-section specimens approximately $0.2D$ in length. Approximately 20 specimens were obtained from each internode and all specimens are obtained from three or four adjacent internodes. In this way it can reasonably be assumed that there is little variation in properties among specimens. Importantly, there is little variation in D and t among the samples used. ‘Clipped’ specimens (Figure 4a) had test regions machined using an end mill (Figure 4b). Specimens were machined such that $\alpha \approx 0.20t$ or $0.25t$ and β and γ are in increments of approximately $0.20t$ or $0.25t$ such that the sum $\alpha + \beta +$

$\gamma = t$, the culm wall thickness. This approach divides the culm wall into segments for which the modulus of rupture determined from each segment is calculated from Eq. 6 and is assumed to represent the average value for that segment; the value is then assigned to the centroid of the segment.

$$f_r = 3Pa/(\alpha t_N + \alpha t_S)L^2 \qquad \text{Eq. 6}$$

The machining was controlled such that α and β at both the N and S quadrant are the same in each specimen (as a result, γ may differ slightly based on variation of t in the cross section). All as-tested dimensions were recorded and these are used in individual calculations of specimen capacity. Control specimens were not clipped; thus $\alpha = t$ and $\beta = \gamma = 0$. The results from the control specimens represent the gross cross-section modulus, f_{rC}, against which the clipped-specimen data is normalised.

3. Specimen Materials

Five different bamboo species were tested in this study, *Phyllostachys edulis*, *Phyllostachys bambusoides*, *Phyllostachys meyeri*, *Phyllostachys nigra*, and *Bambusa stenostachya*. All are thin-walled (D/t generally greater than 8) except *B. stenostachya* which is a thick-walled species. All *Phyllostachys* culms were obtained from a commercial importer and were water treated and kiln dried. The *B. stenostachya* was commercially imported from Vietnam and was borax treated.

In order to place the materials reported in this study in the context of the broader literature, standard longitudinal compression and longitudinal shear (so-called “bow-tie” test) tests (ISO 22157:2019) of all species were conducted; the results are reported in Table 2. Bamboo density normalized for 12% moisture content, ρ_{12}, (ISO 22157:2019) is also reported in Table 2. Specimens had been stored in a laboratory environment for some time prior to testing; the moisture content of all specimens at time of testing was between 13% and 15% as measured with an electronic (pin-type) moisture meter (Table 2).

The objective of this study is to assess the effects of through-culm wall fibre distribution. In order to limit – to the extent possible – material variation, all specimens reported in this paper were taken from the lower region of only a few culms coming from the same batch of each species. Test specimens were cut from within 2 m of each other and included $0.2D$ long specimens for flat ring flexure and $1.0D$ long specimens for compression and longitudinal shear testing. Adjacent samples were used for control and clipped specimens. At least 30 control specimens were tested for each species and as many as 6 specimens of each clipped case were tested (n in Tables 3 and 4). Average culm diameter, D, and wall thickness, t, for each group of samples are reported with the summary of test results in Tables 3 and 4.

3.1 Fibre Distribution

Seven full-culm cross sections (four for *B. Stensostachya*) were selected and digital images were taken at each of the four quadrants (N, S, E and W). These images were processed using a purpose-built MatLab script to obtain the distribution of fibres through the wall cross section. An example of a collected image and resulting MatLab pixel map is shown in Figure 5. The collected images are square, having a dimension equal to the culm-wall thickness, *t* (Figure 5a). The image is divided in the through-thickness direction into ten equal regions of thickness *t/10* (Figure 5b) and the fibre volume ratio obtained for each (Figure 5c). From this analysis, the average fibre distribution (expressed as third-order polynomial best-fit curves) is obtained as summarised at the bottom of Table 1 in terms of the normalised culm wall thickness, x ($x = 0$ is the inner culm wall and $x = 1$ is the outer culm wall). The coefficient of variation of measured fibre volume ratios was less than 0.18 for all but *P. nigra*, which exhibited a COV = 0.24. The 28 *P. edulis* samples shown in Figure 5c have a COV = 0.13. The best-fit equations representing fibre volume distribution reported in Table 1 all have a coefficient of determination $R^2 = 0.99$.

The fibre distribution among the four thin-wall *Phyllostachys* species is very similar. Indeed, a single relationship could be given for all four species having $R^2 = 0.96$ as shown in Table 1. A marked difference in fibre distribution is observed in the thick-walled *B. stenostachya*. Thus, fibre distribution is observed to differ by genera (*Phyllostachys* and *Bambusa*) but less so among species in the same genera (*Phyllostachys*).

4. Full-wall Thickness Flat-Ring Flexure Test Results

Modulus of rupture, f_{rC}, (Eq. 5) determined for the full-culm control specimens is reported in Table 3. Within the genus *Phyllostachys*, these values are similar and notably greater than that observed for *B. stenostachya*. Observed variation of test results is typical of bamboo and similar to that reported in Virgo et al. [2017]. As recommended by Virgo et al., only specimens failing within the constant moment region (Figure 3a) are included in the reported data. Additionally, outliers defined as data falling outside 1.5 times the interquartile range (so called Tukey fences (Hoaglin 2003)), were excluded from the reported data.

5. Clipped Flat-ring Test Results

Experimentally determined values of normalised f_r/f_{rC} determined from the clipped tests are shown in Figure 6 and the corresponding best fit second-order polynomial relationships are reported in Table 3. These all illustrate a similar trend although *P. nigra* specimens exhibit relatively little variation through the culm wall compared to the other species. With the clipped specimens, all failures occurred in the clipped region and no data was determined to be an outlier.

6. Effect of Outer Layer of Bamboo Culm

Integrating the f_r/f_{rC} best-fit curves (Table 3) from $x = 0$ to $x = 1$ should represent the gross modulus across the section; that is, the integral $\int f_r/f_{rC}dx$ should equal unity. However, as shown in Table 3, with the exception of *P. meyeri*, the gross modulus obtained by integrating the clipped data exceeds unity by as much as 20%. A possible explanation for this behaviour – one in which the sum of the parts exceeds the capacity of the whole – is that failure of the full wall section control specimens is being initiated by a ‘weak link’. A brittle failure of the outer layer of the culm wall initiating failure would explain this observation.

The extreme outer layer of a bamboo culm consists of a silica-rich outer skin (epidermis) and a thin region of densely packed fibres (this can be seen at the top of Figure 5). It is believed that this layer will be more brittle than the rest of the culm wall and may help to initiate failures in specimens in which the outer wall is included. Therefore in the clipped specimen testing a question arises: *is the outer layer contributing disproportionately to the observed behaviour, especially to the control and $\beta = 0$ tests*? To investigate this effect, additional specimens were tested having $\beta \approx 0.05t$ and $\alpha \approx 0.95t$ (i.e. $\gamma = 0$, see Figure 4a); essentially, these are full-culm sections with only the outer layer ‘shaved’ away.

Twenty flat-ring flexure specimens were cut from comparable samples of each species tested in the clipped test program (*P. edulis* was not included as there were no comparable specimens available). Alternating specimens along the culm were prepared using a belt sander such that $\beta \approx 0.05t$ and $\alpha \approx 0.95t$ (Figure 4a). Resulting wall thicknesses in the constant moment region are reported in Table 4. Apart from specimen preparation, all tests were identical to those reported previously. To assess potential changes in specimen ductility, displacement of the applied load, δ, was measured and reported at failure of each specimen. Results are presented in Table 4. Also shown in Table 4 is the p-value determined from an unpaired t-test for each set of ‘shaved’ and unshaved specimen. The p-value is the probability that there is no statistically significant difference between the compared conditions.

It is seen that the modulus of rupture, f_r, is essentially unaffected by the removal of the outer layer. With the exception of *P. nigra*, the displacement at failure is observed to increase upon the removal of the outer layer. This increase is greater than can be attributed to the loss of 5% of the moment of inertia of the cross section (resulting from shaving the specimen) alone. To consider the observed behaviour in a normalised fashion, the tangent ‘stiffness’, f_r/δ is also calculated. As seen in Figure 7, specimen stiffness (represented as linear best-fit line in Figure 7) falls on the order of 15 to 30% (with the exception of *P. nigra*) despite the moment of inertia being reduced only 5%. The modulus of rupture itself remains unchanged.

7. Discussion of Observed Transverse Behaviour

The data shown in Figure 6 and equations reported in Table 3 indicate a generally parabolic distribution of modulus of rupture through the culm wall thickness with higher values at both the inner and outer walls and a minimum near the middle of the wall thickness. The fibre volume distributions, also shown in Figure 6 and given in Table 1, indicate a typically observed distribution having few fibres at the inner wall and a greater volume fraction at the outer wall. Based on these fibre distributions, the predicted distribution of modulus of rupture using the Halpin-Tsai equation (Equation 3) does not appear to capture the experimentally observed behaviour, particularly in the inner half of the culm wall where fibre volumes are lowest. Bamboo does not appear to be behaving as a classic fibre-reinforced composite material in the direction transverse to the fibres.

The observed behaviour requires further study and may represent a material variation or morphological variation through the bamboo culm wall thickness. To investigate this further, the failure planes of full-culm wall thickness control specimens were investigated using a scanning electron microscope (SEM). Figure 8 shows an SEM image of a typical *P. edulis* vascular bundle (near the outer culm wall) showing the fibre bundles comprised of microfibrils surrounding the vessel and the parenchyma into which the bundle is embedded. In Figure 8, the fibre bundle can be seen to be penetrated by intra-fibril cracks whereas the interfaces between fibres and parenchyma appear quite intact. It is noted that the parenchyma cell walls are relatively thick indicating a relatively mature culm age [at harvest] (Liese and Weiner 1996). The cracking of the fibres may therefore be a function of culm age (observed although not described by Liese and Weiner). The age at harvest of the bamboo used in this study is unknown and without comparative images, age cannot be estimated. Liese and Weiner (1996), however clearly describe and Liese (1998) illustrates the thickening of the parenchyma wall with age. Alternatively, these cracks may have formed as a result of shrinkage associated with drying (desiccation of the vessel) or treatment of the bamboo. Chen et al (2018) clearly describes different behaviour of the parenchyma and interaction between the parenchyma and fibres based on moisture content. Orsorio et al. (2018) argues that these cracks result for extraction and preparation of the SEM sample. Further study will be made to address the source of these cracks – which are relatively commonly seen – as they represent a stress raiser in the adjacent parenchyma and may be the source of cracks in the parenchyma. Such an effect is shown in an image in Chen et al. (2018) although not described by the authors.

Figure 9 shows SEM images taken from the failure plane of a flat-ring flexure test specimen. Each failure plane was divided into a grid and images of each obtained, allowing the entire failure plane to be imaged. The images shown in Figures 9b and 9c are typical of images obtained at the outer and inner walls, respectively, of a *P.edulis* specimen obtained slightly above the neutral axis of the section in flexure (see Figure 9a). Image features did not vary considerably based on their location through the depth of the specimen (dimension L in Figure 9a).

In Figures 9b and 9c the failure plane can be seen to both follow the edge of the fibre bundles but also to go through the bundles themselves – presumably propagating along the cracks observed in Figure 8. In some locations, the failure plane can be seen to expose the vessels (voids) surrounded by the bundle. Where it is seen at the failure plane, the interface between the parenchyma and the fibre bundle appears intact. This supports the observation that the cracks in the fibre bundle initiate cracks in the parenchyma. In such a case the failure plane represents the propagating crack and little damage would be expected at interfaces parallel to the crack plane. Similar behaviour is reported by Chen et al. (2018) as the propagation of cracks through the parenchyma but around the mircofibrils comprising the fibre bundle. Additionally, the parenchyma shown in Figures 9b and 9c, appear to be behaving differently. Near the outer culm wall (Figure 9b), the failure appears to follow the interfaces between parenchyma cells. Near the inner culm wall (Figure 9c), the failure plane often appears to pass through the parenchyma cells (seen as non-intact cell walls in Figure 9c). This observation is typical of all images obtained in this study. Indeed, near the outer culm wall, the parenchyma is occasionally observed to fail in 'sheets' of intact cells as shown in Figure 10a. In other images (Figure 10b) the intact parenchyma close to the inner culm wall appear 'desiccated': the intact cell wall appears to be 'caving in' or concave rather than being slightly convex nearer the outer culm wall (Figure 8). This observation may suggest a gradient in moisture content through the culm wall or a residual effect of moisture gradient during the drying process – recall that the *P. edulis* was kiln-dried. Such a gradient should be expected. The bamboo culm epidermis is relatively impermeable and resistant to wetting whereas the inner culm wall is permeable (Liese 1998, Yao et al. 2011). The effects of moisture content, 0%, 6% and 20%, on parenchyma behaviour of *P. edulis* has been recently reported by Chen et al. (2018) who attribute increased toughness – particularly of the parenchyma matrix, with increased moisture content.

The longitudinal aspect ratio of the parenchyma cells can be seen to be different in the outer (Figure 10a) and inner (Figure 10b) regions of the culm wall. In recent work, Zeng et al. (2019) identified significantly different morphology of parenchyma cell walls through the culm wall thickness of *P. edulis* samples. Near the outer culm wall, parenchyma cell walls were tightly packed laminar structures with little annular space at interstices (Figure 11c). Nearer the inner culm wall, the laminar structure of the cell wall was separating and a larger triangular pore is present at parenchyma cell interstices (Figure 11a). It is unclear how these differences impact the behaviour illustrated in Figure 9 but it is evident that parenchyma is not homogeneous through the cross section. Neither Zeng et al. (2019) nor Liese (1998) provide insight on the source of this inhomogeneity and the present authors can only speculate on its cause, although it does appear to affect the through thickness mechanical behaviour of the culm wall.

8. Conclusion

This study investigated the transverse material property gradient through the bamboo culm wall and attempts to connect the mechanical results to physical observations and phenomena. Most importantly, the study demonstrates that the transverse behaviour is complex and that bamboo does not appear to behave as a classic fibre-reinforced composite material in the direction transverse to the fibres.

In this study, a modification to the flat-ring flexure test specimen, in which only portions of the culm wall cross-section are tested, is used to obtain a measure of the transverse tensile capacity of the bamboo.

Microscopy analyses are used to qualitatively describe the culm wall architecture and to quantitatively assess the failure modes through the culm wall thickness. The following conclusions are made:

1. Fibre volume distribution through the culm wall was best described by third-order polynomial curves and the COV was observed to be on the order of 0.20 in all cases. Fibre distribution and modulus of rupture, f_{rC}, among the four thin-wall *Phyllostachys* species was very similar, while the same values for *B. stenostachya* was markedly different.
2. The gross modulus obtained by integrating the clipped data exceeds the experimentally determined value of f_{rC} by as much as 20%; that is, the sum of the parts exceeds the capacity of the whole culm.
3. The silica-rich epidermal layer of the culm wall appears to disproportionately affect the full-culm modulus, f_{rC}. Full-culm specimens were tested without this layer and the modulus of rupture was essentially unaffected. The stiffness of the specimens tested without the epidermal layer was reduced considerably more than the small reduction in geometry implies.
4. The distribution of fibre volume and modulus of rupture though the culm wall thickness are shown to not be correlated by conventional assumptions of fibre-reinforced composite material behaviour. The Halpin-Tsai equation (Equation 3) does not appear to capture the experimentally observed behaviour, particularly in the inner half of the culm wall where fibre volumes are lowest.

Scanning electron microscopy (SEM) images of the flat-ring flexure tests failure surfaces reveal a complex behaviour that is not consistent with the assumptions of fibre-reinforced composite behaviour. The following is observed:

5. Failure planes generally pass through the fibre bundles, affected by the vessels (voids) contained in the bundles and cracking between individual fibres comprising the bundles. In general, the interface between fibres and parenchyma (matrix) remains intact.
6. Failure within the parenchyma also varies based on location through the culm wall. Near the outer culm wall, the failure appears to follow the interfaces between parenchyma cells however near the inner culm wall, the failure often appears to pass through the parenchyma cells.
7. Morphologic characteristics of the parenchyma are seen to vary through the culm wall thickness although it is unclear how these differences impact behaviour.

Considerably more research is required to understand the source of the variation in parenchyma structure and its effect on mechanical properties of the bamboo culm. The variation may simply be the natural morphology of the bamboo but may also arise from drying, curing and/or treatment processes. While gross section properties are most important for full-culm bamboo construction, variation of properties through the culm wall may be critical to the performance of laminated bamboo products, particularly those employing tangentially cut strips such as glue-laminated bamboo and cross laminated bamboo [Sharma et al. 2015].

Acknowledgements

This research was funded through National Science Foundation Award 1634739 *Collaborative Research: Full-culm Bamboo as a Full-fledged Engineering Material*. Additional support from the 2015 Institute of International Education Global Innovation Initiative Award *Bamboo in the Urban Environment* and the University of Pittsburgh Swanson School Of Engineering *Summer Research Internship Program* is gratefully acknowledged.

References

Amada, S., Ichikawa, T., Munekata, T., Nagase, Y., and Shimizu, H., (1997) Fiber texture and mechanical graded structure of bamboo, *Composites: Part B*, **28B**, 13-20.

Amada, S., Munekata, T., Nagase, Y., Ichikawa, Y., Kirigai, A. and Zhifei, Y. (1996) The mechanical structures of bamboos in viewpoint of functionally gradient and composite materials, *Journal of Composite Materials*, **30**, 800-819.

Arce-Villalobos O.A. (1993) *Fundamentals of the design of bamboo structures*, Master’s thesis, Eindhoven University of Technology, The Netherlands.

Chen G., Luo H., Yang H., Zhang, T. and Li, S. (2018) Water effects on the deformation and fracture behaviors of the multi-scaled cellular fibrous bamboo. *Acta Biomaterialia* **65**, 203-215

Dixon, P.G. and Gibson, L.J. (2014) The structure and mechanics of Moso bamboo material, *Journal of the Royal Society Interface* **11**, 20140321.

Dixon, P.G., Ahvenainen, P., Aijazi, A.N., Chen, S.H., Lin, S., Augusciak, P.K., Borrega, M., Svedstrom, K. and Dixon, L.J., Comparison of the structure and flexural properties of Moso, Guadua and Tre Gai bamboo, *Construction and Building Materials*, **90**, 11-17.

Ghavami, K. and Marinho, A.B. (2005) Propriedades físicas e mecânicas do colmo inteiro do bambu da espécie Guadua angustifolia, *Revista Brasileira de Engenharia Agrícola e Ambiental,* **9**(1), 107-114. (in Portuguese)

Ghavami, K., Rodriques, C.S., and Paciornik, S., (2003) Bamboo: Functionally Graded Composite Material, *Asian Journal of Civil Engineering (Building and Housing)*, **4**(1), 1-10.

Grosser and Liese (1971) On the anatomy of Asian Bamboos, with Special Reference to their vascular bundles. *Wood Science and Technology***,** **5**, 290-312.

Habibi, M.K., Samaei, A.T., Gheshlaghi, B., Lu, J. and Lu, Y. (2015) Asymmetric flexural behaviour from bamboo’s functionally graded hierarchical structure: Underlying mechanisms, *Acta Biomaterialia*, **16**, 178-186.

Halpin, J.C. and Kardos, J.L. (1976) The Halpin-Tsai Equations: A Review, *Polymer Engineering and Science* **16**(5), 344-352.

Harries, K.A., Bumstead, J., Richard, M.J. and Trujillo, D. (2017) Geometric and Material Effects on Bamboo Buckling Behaviour, *ICE Structures and Buildings* Themed issue on bamboo in structures and buildings, **170**(4), 236-249.

Hewitt, R.L. and de Malherbe, M.C. (1970) An Approximation for the Longitudinal Shear Modulus of Continuous Fiber Composites, *Composite Materials*, **4,** 280.

Hoaglin, D.C. (2003) John W. Tukey and Data Analysis, *Statistical Science* **18**(3), 311-318.

ISO 22157:2019 *Bamboo structures -- Determination of physical and mechanical properties of bamboo culms -- Test methods*. International Organization for Standardization

Janssen, J. (1981) *Bamboo in Building Structures*. Doctoral Dissertation, Eindhoven University of Technology, Netherlands.

Janssen, J.J.A., (2000) *Designing and Building with Bamboo*, INBAR Technical Report 20. International Network for Bamboo and Rattan, Beijing, China.

Krause, J.Q., Andrade Silva, F., Ghavami, K., Gomes, O.F.M, Toledo Filho, R.D., On the influence of Dendrocalamus giganteus bamboo microstructure on its mechanical behavior, *Construction and Building Materials*, **127**, 199-209.

Liese, W. (1998) *The Anatomy of Bamboo Culms*, Brill. 204 pp.

Liese, W. and Weiner, W. (1996) Ageing of Bamboo Culms. A Review. *Wood Science and Technology*, **30**, 77-89.

Mallick, P. K. (2008). *Fiber-reinforced composites: materials, manufacturing, and design* (third edition). CRC press.

Mitch, D., Harries, K.A., and Sharma, B. (2010) Characterization of Splitting Behavior of Bamboo Culms. *ASCE Journal of Materials in Civil Engineering* **22**, 1195-1199.

Nogata, F. and Takahashi, H. (1995) Intelligent functionally graded material: bamboo, *Composites Engineering*, **5**, 743-751.

Osorio L., Trujillo E., Lens F., Ivens, J. Verpoest, I. and Van Vuure, AW., (2018) In-depth study of the microstructure of bamboo fibres and their relation to the mechanical properties. *Journal of Reinforced Plastics and Composites* **37**, 1099-1113

Richard, M. (2013) *Assessing the Performance of Bamboo Structural Components*, Doctoral Dissertation, University of Pittsburgh.

Richard, M., Gottron, J., Harries, K.A. and Ghavami. K. (2017) Experimental Evaluation of Longitudinal Splitting of Bamboo Flexural Components, *ICE Structures and Buildings* Themed issue on bamboo in structures and buildings, 170(4), 265-274

Richard, M.J., Harries, K.A., (2015) On Inherent Bending in Tension Tests of Bamboo, *Wood Science and Technology* **49**(1) 99-119.

Shao, Z.P., Zhou, L., Liu, Y.M., Wu, Z.M. and Arnauld, C. (2010) Differences in structures and strength between internode and node sections of Moso bamboo, *Journal of Tropical Forest Science*, **22**(2), 133-138.

Sharma B, Gatoo A, Bock M, Ramage M (2015) Engineered Bamboo for structural applications. *Construction and Building Materials*, **81**, 66-73.

Sharma, B., Harries, K.A. and Ghavami, K. (2012) Methods of Determining Transverse Mechanical Properties of Full-Culm Bamboo, *Journal of Construction and Building Materials*, **38**, 627-637.

Sharma, B. and Harries, K.A. (2012). Effect of Fiber Gradation on the Edge Bearing Strength on Bamboo Culms, *Key Engineering Materials*, Vol 517, pp 63-70.

Tan, T., Rahbar, N., Allameh, S.M., Kwolfie, S., Dissmore, D., Ghavami, K. and Soboyejo, W.O. (2011) Mechanical Properties of functionally graded hierarchical bamboo structures, *Acta Biomaterialia* **7**, 3796-3803.

Vaessen, M.J. and Janssen, J.A. (1997) Analysis of the critical length of culms of bamboo in four-point bending tests, *HERON*, **42**(2), 113-124.

Virgo, J., Moran, R., Harries, K.A., Garcia, J.J., and Platt, S. (2017) Flat Ring Flexure Test for Full-Culm Bamboo, *Proceedings of 17th International Conference on Non-Conventional Materials and Technologies (17NOCMAT)*, Yucatán, México, November 2017.

Yao, L.H., Wang, X.M. and Fei, B.H. (2011) Study on Permeability Coefficient of Different Bamboo/Fir Veneer Surface, *Advanced Materials Research*, **311-313**, 1634-1637.

Zeng, Q., Zhang, Q., Lu, Q., Zhou, Y., Chen, N., Rao, J. and Fan, M. (2019; in press) Wetting behavior and laminate bonding performance of profiled tangential surfaces of moso bamboo, *Industrial Crops and Products*

Table 1 Summary of through-culm wall fibre volume and modulus distributions.

ref[1]	method[2]	species	B M T[3]	gross section		interior ($x = 0$)		exterior ($x = 1$)		proposed relationship
				V_f	E_L (GPa)	V_f	E_L (GPa)	V_f	E_L (GPa)	
1, 2	IA	general	nr	0.40	-	0.20	-	0.60	-	$V_f = 0.40x + 0.20$
3	V_f: IA E_L: RoM	*P. edulis*	B	-	9.1	0.09	2.5	0.77	22.6	exponential V_f $E_L = (E_{L,x=0})e^{2.2x}$
			T	-	13.7	0.11	3.8	0.88	33.8	
4	V_f: IA E_L: tens	*P. edulis*	B	0.25	-	0.17	4	0.50	29	exponential V_f and E_L
			M	0.28	-	0.18	6	0.56	30	
			T	0.34	-	0.10	6	0.60	32	
5	IA	*P. edulis*	nr	0.28	-	0.12	-	0.62	-	$V_f = 0.49x^2 + 0.0066x + 0.12$
5	IA	*D. giganteus*	B	0.42	-	0.29	-	0.53	-	$V_f = -0.09x^2 + 0.33x + 0.29$
			M	0.43	-	0.21	-	0.62	-	$V_f = 0.07x^2 + 0.29x + 0.26$
			T	0.43	-	0.19	-	0.60	-	$V_f = -0.12x^2 + 0.51x + 0.21$
6	V_f: SEM E_L: tens	*G. angustifolia*	B	0.26	16.0	0.19	-	0.62	-	$V_f = 0.83x^2 – 0.41x + 0.19$
			M	0.26	14.6	-	-	0.54	-	$V_f = -1.02x^3 + 2.61x^2 – 1.38x + 0.33$
			T	-	13.2	-	-	0.54	-	$V_f = -4.13x^4 + 9.68x^3 – 6.68x^2 + 1.71x – 0.04$
7	tens	*P. edulis*	M	-	-	0.12	4.5	0.54	21	$E_L = 40.13V_f + 0.22$
8	nano	*P. edulis*	nr	-	-	-	6.5	-	13.8	none reported
9	SEM	*P. edulis*	B	0.21	-	0.06	-	0.52	-	$V_f = (0.23x + 0.71)(0.09e^{1.83x})$
			M	0.23	-	0.06	-	0.58	-	$V_f = (0.23x + 0.71)(0.09e^{1.48x})$
			T	0.26	-	0.06	-	0.69	-	$V_f = (0.23x + 0.71)(0.09e^{2.11x})$
10	V_f: SEM E_L: nano	*P. edulis*	nr	-	14.9	0.07	-	0.58	-	none reported
		G. angustifolia	nr	-	19.7	0.16	-	0.60	-	
		B. stenostachya	nr	-	13.8	0.05	-	0.42	-	
11	flex	*P. edulis*	nr	-	8.7	-	2.8	-	15.2	$E_L = 12.43x^{0.43} + 2.78$
12	V_f: SEM E_L: tens	*D. giganteus*	M	-	-	0.38	17.6	0.55	30.7	culm wall divided into thirds
		at $x = 0.5$		-	-	0.45	27.3	-	-	
this study	IA	*P. edulis*	B	0.29	-	0.12	-	0.67	-	$V_f = 1.41x^3 – 1.23x^2 + 0.50x + 0.10$
		P. bambusoides	B	0.32	-	0.14	-	0.65	-	$V_f = 0.96x^3 – 0.91x^2 + 0.57x + 0.10$
		P. nigra	B	0.26	-	0.07	-	0.64	-	$V_f = 0.94x^3 – 0.63x^2 + 0.36x + 0.06$
		P. meyeri	B	0.35	-	0.11	-	0.70	-	$V_f = 0.15x^3 + 0.34x^2 + 0.17x + 0.11$
		B. stenostachya	B	0.35	-	0.24	-	0.64	-	$V_f = 1.75x^3 – 1.98x^2 + 0.75x + 0.20$
		all four Phyllostachys	B	-	-	-	-	-	-	$V_f = 0.86x^3 – 0.61x^2 + 0.40x + 0.09$

x = normalized dimension through culm wall; V_f = fibre volume ratio; E_L = longitudinal tensile modulus of elasticity

[1] references: 1 = Janssen 1981; 2 = Vaessen and Janssen 1997; 3 = Nogata and Takahasi 1995; 4 = Amada et al. 1996; 5 = Ghavami et al. 2003; 6 = Ghavami and Marhinho 2005; 7 = Shao et al. 2010; 8 = Tan et al. 2011; 9 = Dixon and Gibson 2014; 10 = Dixon et al. 2015; 11 = Habibi et al. 2015; 12 = Krause et al. 2016

[2] methods of determining data: IA = image analysis; SEM = scanning electron microscope; RoM = rule of mixtures; tens = tension tests; nano = nanoindentation; flex = flexural tests

[3] locational along height of culm: B = bottom; M = middle; T = top; nr = not reported

Table 2 Mechanical properties bamboo used in this study (COV in parentheses).

species	density at 12% MC, ρ_{12}	moisture content at time of test	compressive strength, f_c	longitudinal shear strength, f_v
	kg/m^3	%	MPa	MPa
P. edulis	896 (0.01)	14.0	48.1 (0.20)	15.1 (0.11)
P. bambusoides	818 (0.04)	14.6	59.3 (0.26)	14.6 (0.22)
P. nigra	907 (0.02)	14.8	45.2 (0.13)	14.6 (0.16)
P. meyeri	840 (0.04)	13.7	55.8 (0.11)	16.4 (0.05)
B. stenostachya	616 (0.03)	13.0	46.0 (0.21)	9.9 (0.11)

Table 3 Summary of experimental results on clipped specimens (COV in parentheses).

species	full-culm control specimens				clipped specimens				
	n	D	t	f_{rC}	n	D	t	f_r/f_{rC}	$\int \frac{f_r}{f_{rC}} dx$
		mm	mm	MPa		mm	mm		
P. edulis	33	117 (0.06)	10.1 (0.10)	17.3 (0.18)	13	112 (0.05)	9.5 (0.09)	$4.0x^2 – 4.9x + 2.3$ ($R^2 = 0.82$)	1.18
P. bambusoides	27	95.5 (0.05)	8.2 (0.22)	15.7 (0.21)	14	94.8 (0.06)	8.1 (0.24)	$2.6x^2 – 2.5x + 1.5$ ($R^2 = 0.31$)	1.12
P. nigra	31	93.5 (0.03)	6.7 (0.19)	15.6 (0.14)	16	92.4 (0.01)	6.5 (0.14)	$0.7x^2 – 0.8x + 1.4$ ($R^2 = 0.08$)	1.23
P. meyeri	49	65.3 (0.12)	6.6 (0.10)	20.0 (0.16)	20	65.2 (0.09)	6.4 (0.11)	$2.4x^2 – 1.8x + 1.1$ ($R^2 = 0.59$)	1.00
B. stenostachya	39	77.5 (0.06)	14.5 (0.32)	9.4 (0.13)	17	75.4 (0.06)	14.7 (0.28)	$4.1x^2 – 3.6x + 1.6$ ($R^2 = 0.77$)	1.17

Table 4 Summary of results from specimens having outer layer removed (COV in parentheses).

species	n	D	t	modulus of rupture, f_r		deflection, δ		f_r/δ	
		mm	mm	MPa	p[1]	mm	p[1]	MPa/mm	p[1]
P. bambusoides	10	99.6 (0.01)	6.47 (0.09)	18.1 (0.08)	0.09	1.86 (0.13)	0.00	9.9 (0.14)	0.01
outer layer removed	10	99.8 (0.01)	$0.92t$ (0.04)	19.7 (0.12)		2.30 (0.16)		8.4 (0.08)	
P. nigra	10	96.0 (0.01)	8.44 (0.03)	26.4 (0.16)	0.75	2.10 (0.09)	0.59	12.6 (0.15)	0.99
outer layer removed	9	95.8 (0.01)	$0.95t$ (0.02)	26.0 (0.06)		2.06 (0.06)		12.6 (0.06)	
P. meyeri	4	62.8 (0.00)	6.58 (0.02)	22.5 (0.08)	0.22	0.95 (0.20)	0.06	25.0 (0.33)	0.09
outer layer removed	5	62.9 (0.01)	$0.95t$ (0.02)	21.0 (0.07)		1.21 (0.14)		17.6 (0.14)	
B. stenostachya	7	71.7 (0.02)	15.00 (0.03)	13.8 (0.10)	0.86	1.59 (0.22)	0.10	9.3 (0.30)	0.13
outer layer removed	9	72.2 (0.02)	$0.95t$ (0.04)	14.0 (0.09)		1.91 (0.18)		7.6 (0.17)	

[1] p-values indicate the probability that there is no statistical difference between the compared samples

a) longitudinal section of bamboo culm showing portions of internodes to either side of node

b) cross section of culm near node diaphragm

c) section through culm wall

d) vascular bundle

Figure 1 Anatomy of bamboo culm showing functionally graded distribution of fibre in culm wall [adapted from Richard 2013].

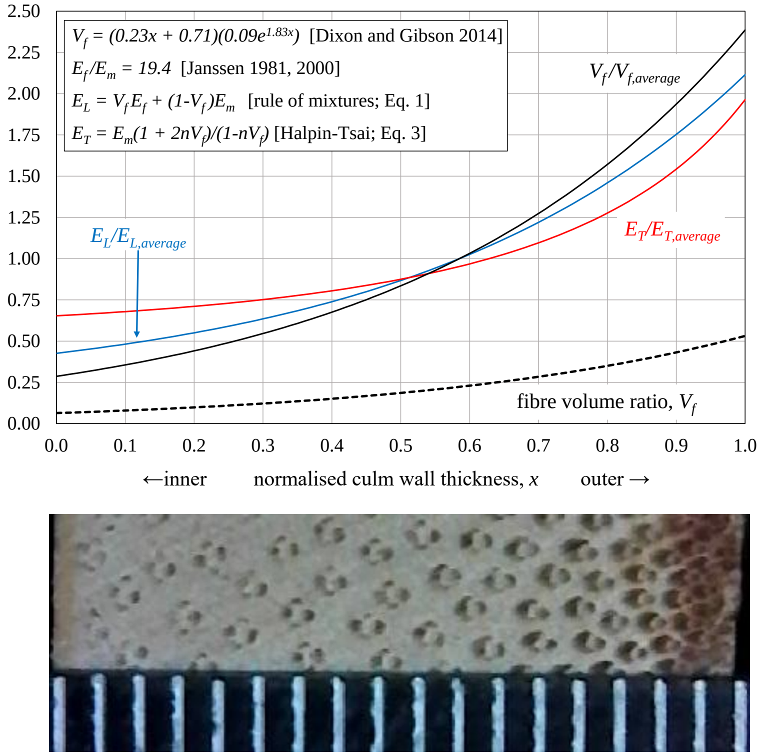

Figure 2 Distribution of fibres and modulus through culm wall based on rule of mixtures.

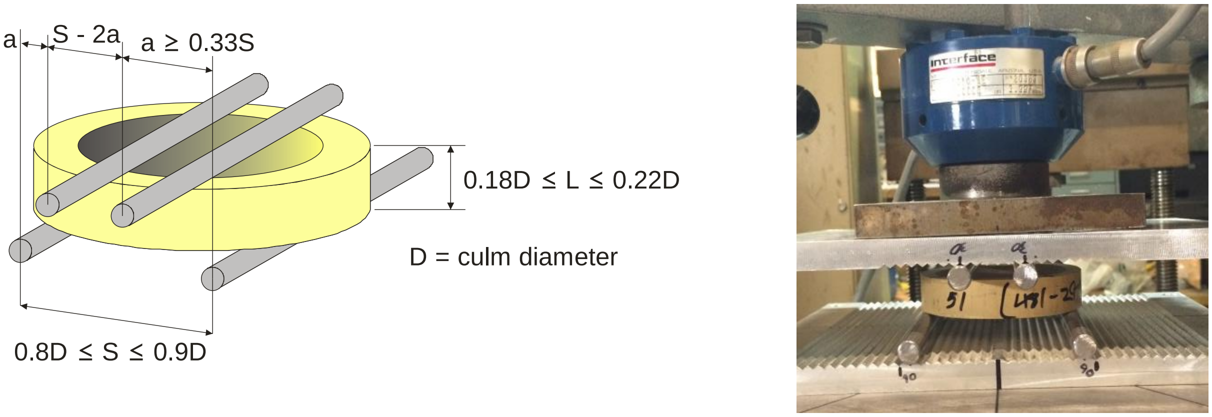

a) test set-up schematic and dimensions

b) test being conducted in universal test machine (shown: 100 mm diameter culm tested over 80 mm span with 25 mm shear span)

Figure 3 Flat ring flexure test.

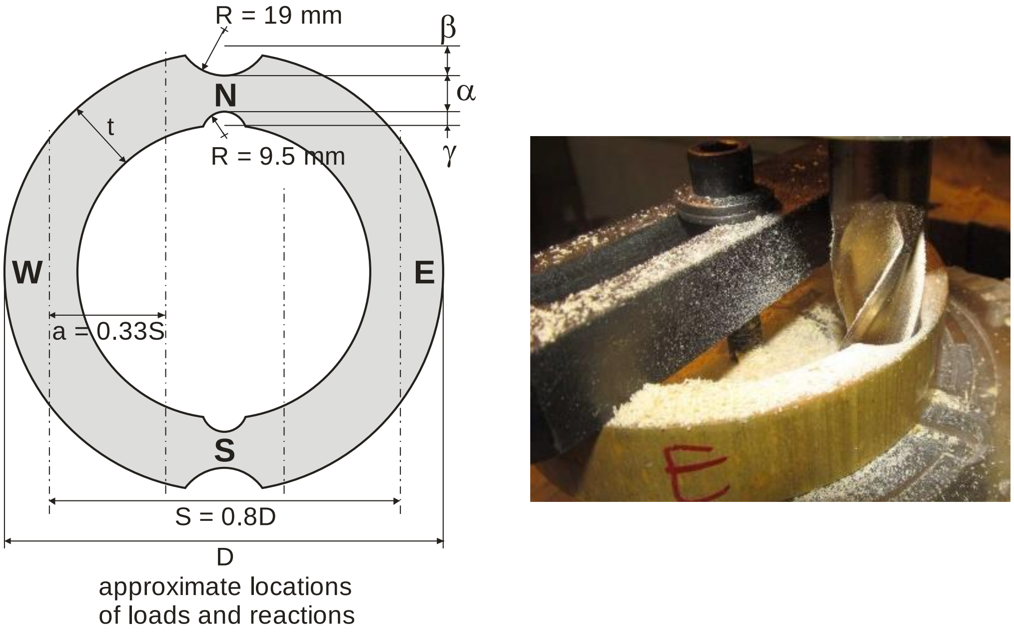

a) test specimen schematic and dimensions

b) specimen machining (shown: $\beta = 0$, $\alpha = 0.20t$ and therefore, $\gamma = 0.80t$)

Figure 4 Flat ring flexure specimen.

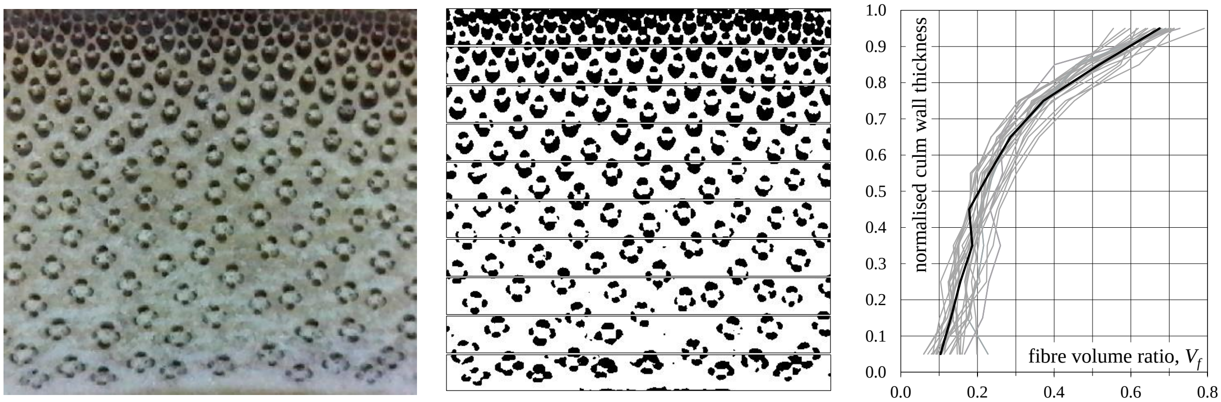

a) image of culm wall

b) MatLab pixel map of fibres divided into ten layers

c) fibre volume distribution for 28 *P edulis* samples, Black line corresponds to image in figures a) and b)

Figure 5 Example of digital image analysis of culm wall (*P.edulis* sample shown)

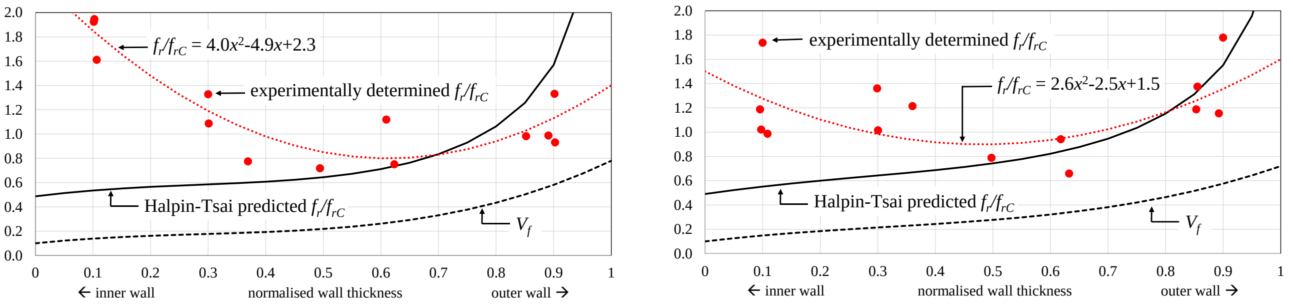

a) *P. edulis* b) *P. bambusoides*

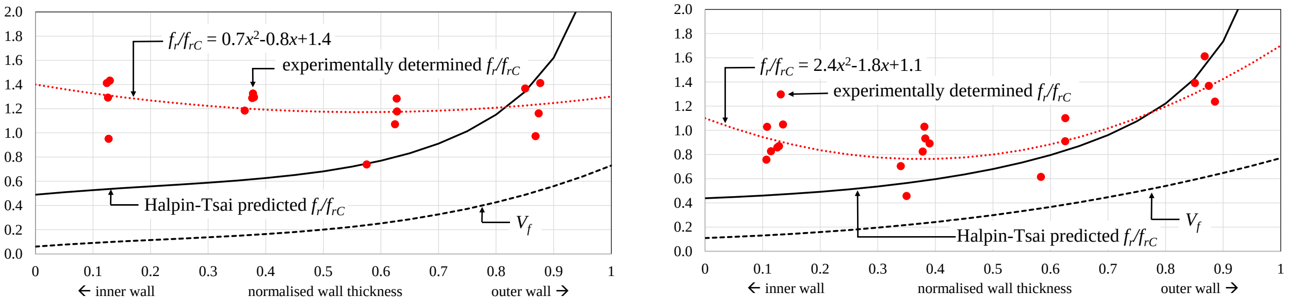

c) *P. nigra* d) *P. meyeri*

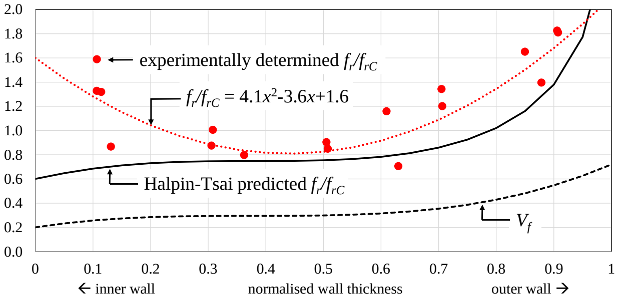

e) *B. stenostachya*

Figure 6 Variation of modulus of normalised rupture through culm wall section.

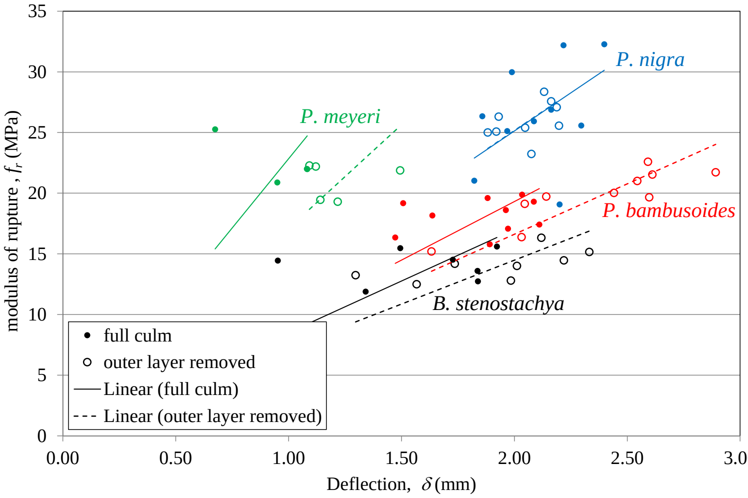

Figure 7 Comparison of full-culm specimens and those having only outer layer removed.

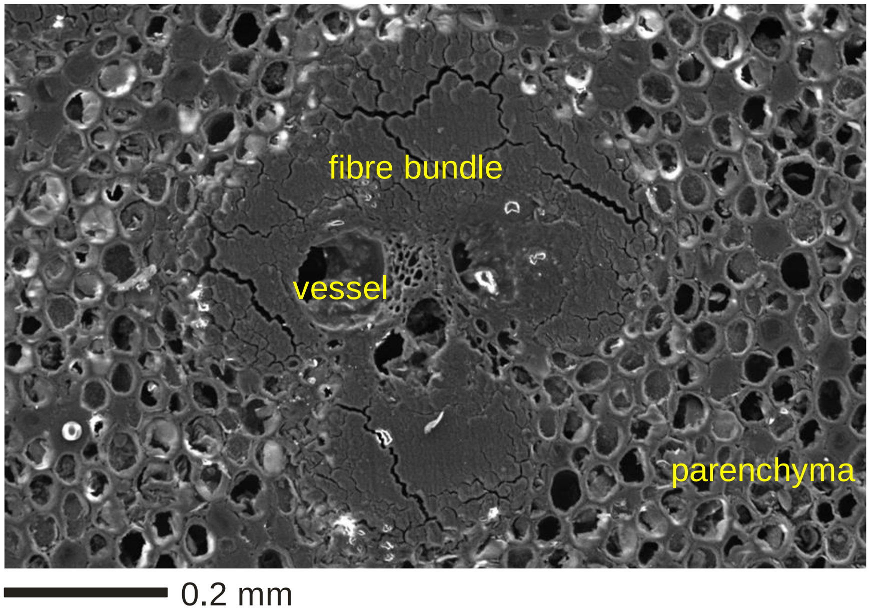

Figure 8 SEM image of *P.edulis* vascular bundle

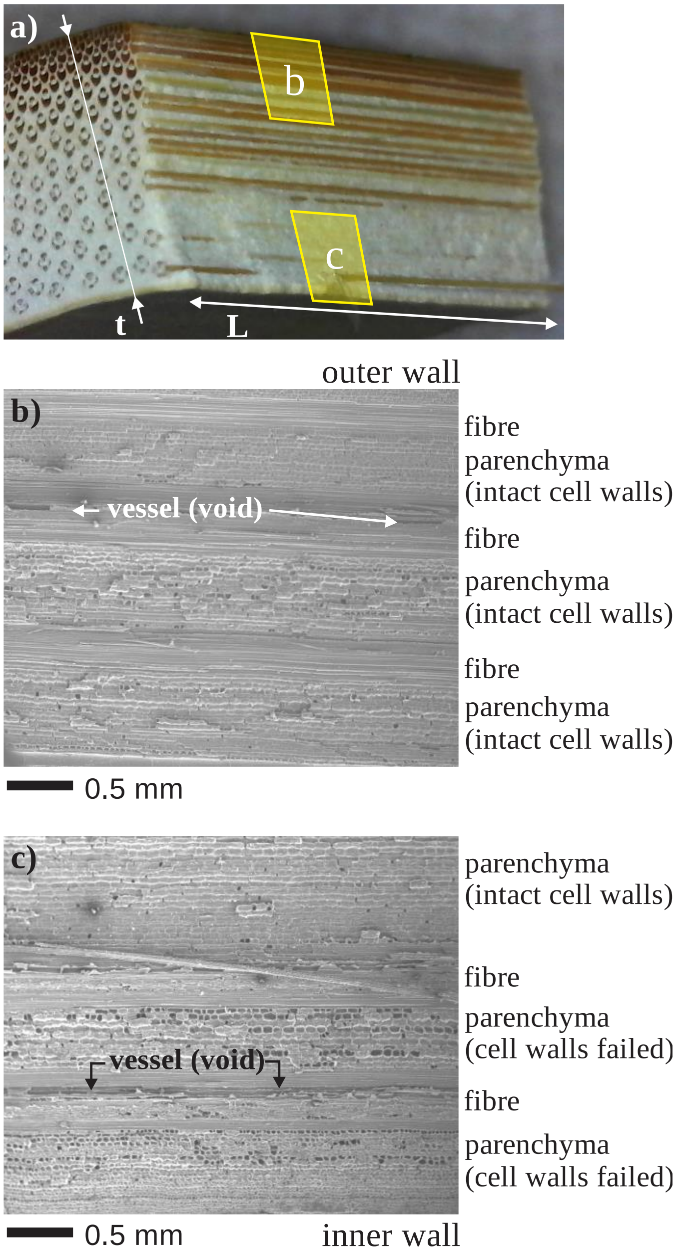

Figure 9 Detail of culm wall images of *P. edulis* specimen
(note that images in parts b and c are not the same specimen as shown in a)

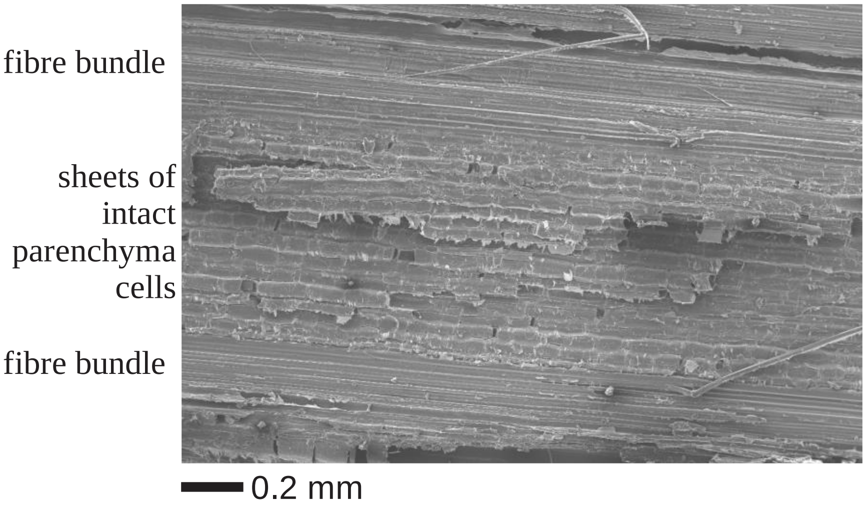

a) parenchyma between two fibre bundles near outer culm wall

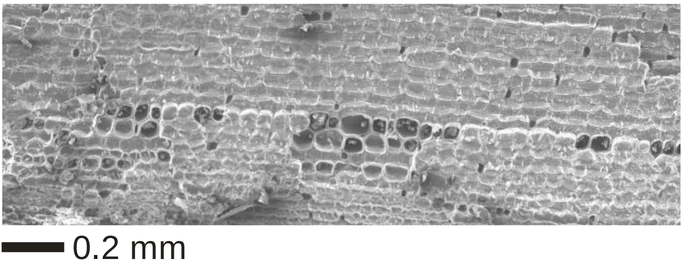

b) parenchyma near inner culm wall

Figure 10 SEM images of *P. edulis* parenchyma.

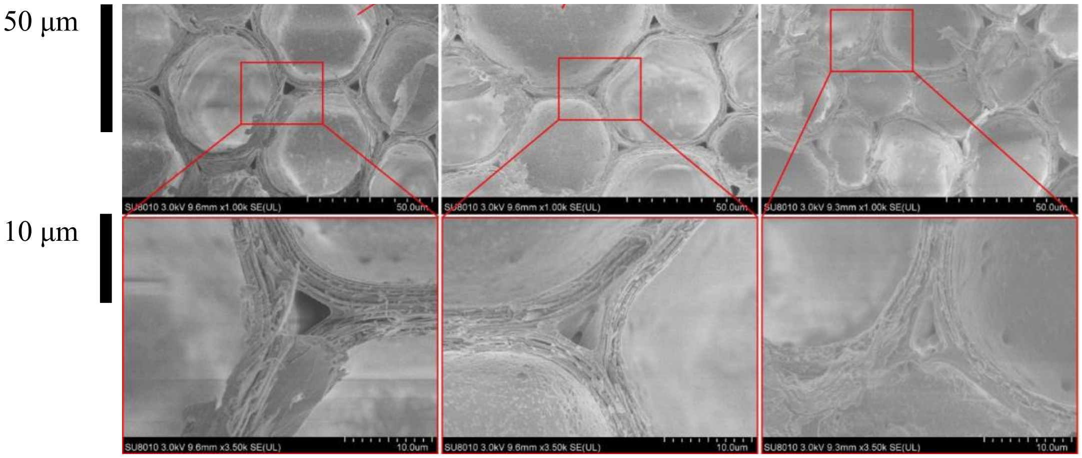

a) near inner culm wall b) middle of culm wall c) near outer culm wall

Figure 11 SEM images of parenchyma cell wall interstices (Zeng et al. 2019)